Acta Crystallographica Section A
Foundations of Crystallography
ISSN 0108-7673

Received 29 January 2004
Accepted 7 July 2004

High-resolution synchrotron data collection for charge-density work at 100 and 20 K

Peter Luger,[a]* Marc Messerschmidt,[a] Stephan Scheins[a] and Armin Wagner[b]

[a]Institute for Chemistry/Crystallography, Free University Berlin, Takustrasse 6, D-14195 Berlin, Germany, and [b]Paul Scherrer Institute, 5232 Villingen PSI, Switzerland. Correspondence e-mail: luger@chemie.fu-berlin.de

For the measurement of very accurate high-resolution X-ray data for charge-density work, synchrotron beamlines provide a bright radiation source of outstanding properties. Most important are the very high primary intensity and the possibility of choosing hard radiation with $\lambda \approx 0.5$ Å or even shorter. This together with area detection and a stable low-temperature device means that accurate and large data sets can be measured in a short time. A number of data collections are reported, which were carried out at the beamlines F1 and D3 of Hasylab (DESY, Hamburg) first at 100 K and later at 15–20 K, demonstrating the quality of the measured intensities. A low temperature of around 20 K was obtained at beamline D3 with a double-stage closed-cycle helium cryostat where the standard beryllium cylinder of the vacuum chamber was replaced by a 0.1 mm Kapton film. Comparison of different data sets measured for a strychnine crystal demonstrated how I/σ ratios favorably improve if synchrotron radiation at a low temperature of 15 K was used. Synchrotron-based studies on several biologically active compounds are briefly summarized and a synchrotron experiment of an otherwise not sufficiently diffracting crystal of a tetraphenyl barbaralane derivative is described in detail. Atomic volumes and charges of a highly substituted C_{60} fullerene are reported derived from a synchrotron data set of more than 350000 reflections.

1. Introduction

For experimental charge-density determinations, a number of strict requirements have to be fulfilled. Among them is the necessity to measure very accurate X-ray data even in the higher regions of reciprocal space and to maintain the lowest possible temperature during data collection.

With these experimental conditions, synchrotron beamlines provide a bright source for X-radiation of outstanding properties. Most important for charge-density experiments are the very high primary intensity and the tuneable wavelength allowing a choice of $\lambda \approx 0.5$ Å or even shorter. This enables high-resolution data sets to be collected, if needed, also for smaller crystals, allowing absorption and extinction problems to be minimized. If, in addition, a sensitive modern area detector and a stable low-temperature device are available, accurate and large data sets can be measured in a short time. However, as pointed out by others (Dauter, 2002), there are pros and cons to consider. Among the cons are, depending on the storage-ring conditions, various beam instabilities, needing careful and time-consuming corrections. Sometimes even worse is the narrow time scale of a beam time period making it in practice impossible to correct for inadequate crystal quality or to overcome failures occurring in the beamline set-up.

We shall report here on our experiences with a number of charge-density data collections carried out at the beamlines F1 and D3 of Hasylab (DESY, Hamburg) first at 100 K and later at 20 K, demonstrating the quality of the measured intensities and showing that in a number of cases synchrotron radiation is essential for a successful charge-density determination.

1.1. Experimental set-up

The set-ups we have been using are the four-circle diffractometer at beamline D3 consisting of the large Huber Eulerian cradle (400 mm diameter) with offset χ circle and the κ-axis diffractometer at beamline F1, both operated with vertical diffraction geometry. In both cases, an Si(111) double-crystal monochromator allows the wavelength to be tuned from longer wavelengths to below 0.5 Å. We made no attempt to choose $\lambda < 0.5$ Å since for our compounds with some sizable lattice constants there was the danger of losing strong low-order reflections behind the beam stop. Area detection could be made available at both beamlines with a Bruker Smart 1K detector and corresponding software.

Sample cooling down to 100 K was normally achieved by using conventional and commercially available nitrogen-gas-

stream devices. It has been shown, however (Zobel *et al.*, 1992; Williams *et al.*, 1999; Koritsanszky *et al.*, 2000), that a significant and hence favorable reduction of thermal motion takes place when the temperature is further lowered to 10–20 K. This can in principle be achieved by replacing nitrogen with helium in the open-flow gas-stream devices, however, the open-flow helium systems are not affordable for normal university laboratories because of the high running costs with respect to helium consumption. A low running-cost alternative is a closed-cycle helium cryostat. So we invested some efforts to realize this option at the D3 beamline, more so since a double-stage cryostat was available and could be mounted on the diffractometer thanks to its special geometry (Fig. 1).

The technical problem of the vacuum chamber to be used around the cold head of the cryostat was solved as described recently (Messerschmidt *et al.*, 2003) in that beryllium was replaced by a kapton film as cylinder-wall material of the vacuum chamber. This results in a significantly lower and practically unstructured background and makes this closed-cycle cryostat applicable in combination with a modern area detector. Hence the temperature range for data collection can be extended to around 15–20 K. In a first comparative study on several high-order data sets of strychnine single crystals at 100 and 15 K, it was demonstrated that I/σ ratios of high-order reflections improved most favorably if synchrotron radiation at a temperature of 15 K was used (Messerschmidt *et al.*, 2003). As shown in Fig. 2, the I/σ curves decrease drastically at medium sin θ/λ values, say 0.8 Å^{-1}, for two 100 K data sets measured with conventional X-ray sources. The situation improves for a 15 K Mo $K\alpha$ data set, but is best for the synchrotron data set measured at 15 K, where the I/σ decrease is moderate even far beyond sin $\theta/\lambda > 1.0$ Å^{-1}.

Figure 1
Huber four-circle diffractometer at beamline D3 (Hasylab) equipped with He cryostat and Smart 1K CCD area detector. The vacuum chamber wall at the cold head of the cryostat is made of Kapton film.

2. Applications

In the following sections, we give a brief overview of a number of charge-density studies we have performed in the field of biologically important compounds based in most cases on synchrotron experiments. It will be followed by a more detailed description of results from a charge-density study of a barbaralane derivative and we will discuss atomic properties of a highly substituted C_{60} fullerene derivative.

2.1. Charge-density studies on biologically active compounds

It was shown for the first time in the mid-nineties that the combination of synchrotron radiation and CCD area detection yielded sufficiently accurate data sets for charge-density work. This set-up reduced the time-consuming nature of the high-resolution X-ray diffraction experiment to one or a few days (Koritsanszky *et al.*, 1998) so that the perspective was open either to enter into comparative charge-density studies on an entire class of chemically related compounds or to work on larger compounds, for example those of biological relevance.

Both routes were followed. The class of 20 genetically encoded amino acids was the first one where comparative topological data from experimental charge densities were obtained. Until now, results of 14 of the 20 compounds have been published (Gatti *et al.*, 1992; Coppens *et al.*, 1999; Destro *et al.*, 2000; Arnold *et al.*, 2000; Flaig *et al.*, 2002; Scheins *et al.*, 2004). Synchrotron radiation was favorably applied to collect data sets to very high resolution of sin $\theta/\lambda > 1.4$ Å^{-1} for some samples [DL-Ser, DL-Val, L-Asn·H_2O, see Flaig *et al.* (2002)]. Bader's group has published topological and atomic properties of all 20 amino acids based on theoretical calculations (Matta & Bader, 2000, 2002, 2003), so that this class of compounds is the first one where a complete set of theoretical charge-density data is available and where the corresponding experimental studies are approaching completeness.

In our group, the work on larger molecules was directed to investigations on oligopeptides and pharmaceutically active compounds, where recently a study on active and inactive

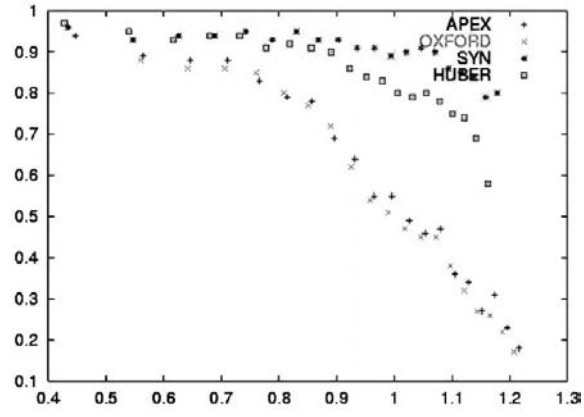

Figure 2
I/σ ratios plotted against sin θ/λ (Å^{-1}) for four high-resolution data sets of strychnine. APEX and OXFORD are 100 K Mo $K\alpha$ data sets, HUBER is a 20 K Mo $K\alpha$ data set and SYN is a 15 K data set measured at beamline D3 of Hasylab (see also Messerschmidt *et al.*, 2003).

penicillin derivatives was finished (Wagner *et al.*, 2004). This made it possible not only to compare an increasing sample of bond topological properties but later submolecular partitions could be applied making use of the zero flux surfaces in the electron-density gradient vector field. This enabled the derivation of atomic properties and the study of transferability and additivity of chemically comparable fragments, a key concept in Bader's theory of 'atoms in molecules' (AIM) (Bader, 1990). In most of our studies on larger molecules, synchrotron-radiation experiments performed at beamline F1 and D3 of Hasylab were essential to obtain sufficiently resolved data sets. In one case, of the hexapeptide cyclo-(D,L-Pro)$_2$-(L-Ala)$_4\cdot H_2O$, a comparison of a synchrotron data set and corresponding Mo $K\alpha$ data from a rotating anode could be made (see Dittrich *et al.*, 2002). Results of these studies have already been published elsewhere and will not be elaborated here (Dittrich *et al.*, 2000, 2003; Scheins *et al.*, 2004; Wagner *et al.*, 2004).

2.2. Charge density of 2,4,6,8-tetraphenylbarbaralane (I) at 110 and 20 K

One example where synchrotron radiation was especially useful was the charge-density analysis of 2,4,6,8-tetraphenylbarbaralane (I). Like bullvalene and semibullvalene, barbaralane belongs to the class of cage compounds that undergoes a degenerate Cope rearrangement in solution. This is a special case of the classic Cope rearrangement (Williams, 2001), where a synchronous reorientation of one σ and two π bonds takes place, transferring the molecule into an identical structure but a different connectivity.

Owing to the moderate crystal quality and the low scattering power, synchrotron radiation was essential for measuring reflections up to a resolution of $\sin\theta/\lambda = 1.16$ Å^{-1}. Further details on the crystal data and the experimental conditions are given in Table 1.

Table 1
Crystal and structure refinement data for 2,4,6,8-tetraphenylbarbaralane (I).

Empirical formula	$C_{33}H_{26}$
Formula weight (g mol^{-1})	422.54
Crystal system	Monoclinic
Space group	$C2/c$
Z	8
Temperature (K)	110 (3)
Beamline	F1
Unit-cell dimensions	
a (Å)	26.232 (5)
b (Å)	10.399 (2)
c (Å)	19.618 (4)
β (°)	119.451 (3)
V (Å^3)	4659 (2)
Calculated density (g cm^{-3})	1.205
$F(000)$	1792
λ (Å)	0.56
Absorption coefficient μ (mm^{-1})	0.04
Max. 2θ (°)	81.07
$(\sin\theta/\lambda)_{max}$ (Å^{-1})	1.16
No. of collected reflections	62291
Symmetry-independent reflections	27038
$wR(F)$	0.034
$R_1(F)$	0.032
$R_{all}(F)$	0.046
GoF	1.86

As found earlier at room temperature (Quast *et al.*, 1993), the arrangement of the phenyl rings on the barbaralane skeleton does not satisfy the possible C_s symmetry of the molecule. Fig. 3 shows an *ORTEP* (Burnett & Johnson, 1996) plot of the molecule (50% probability) based on the $T = 110$ K data. One of the four phenyl rings was found to be disordered (C22–C27). This disorder could be easily resolved during conventional spherical-atom refinement and 50% occupancies were kept fixed during multipolar refinement. The multipole parameters of the disordered atoms were constrained to those of the well resolved phenyl ring atoms. Fig. 4 shows a static deformation density map and a residual map of the disordered phenyl ligand. The contour intervals in both figures are 0.05 e Å^{-3}. The residual map shows no significant maxima indicating that the disorder in this region has been properly modelled by the multipole formalism. In Fig. 5, the static deformation density maps of the cyclopropane ring (*a*) and in the C4—C5—C6 plane of the title compound (*b*) are shown.

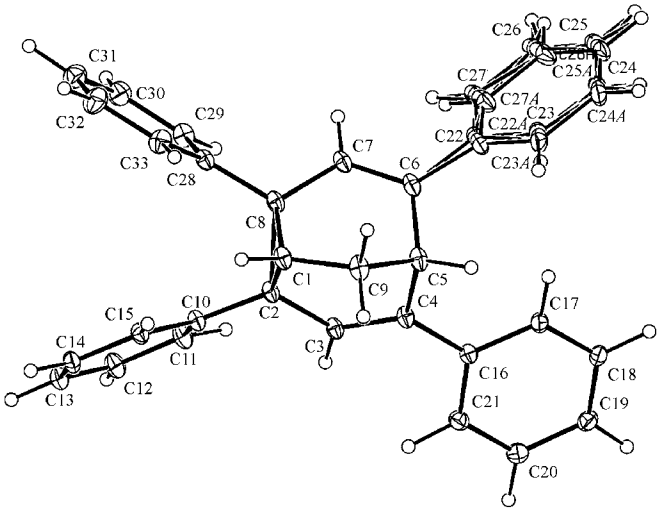

Figure 3
ORTEP (Burnett & Johnson, 1996) representation of 2,4,6,8-tetraphenylbarbaralane (I) (50% probability) at 110 K with atomic numbering.

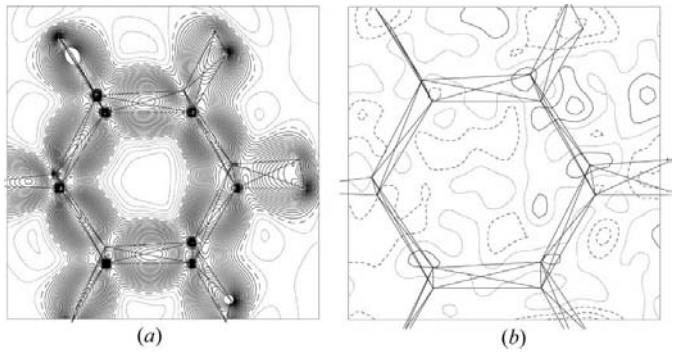

Figure 4
Deformation density map and residual map of the disordered phenyl ring C22–C27 of (I) at 110 K. Contour intervals are 0.05 e Å^{-3}.

Table 2
Comparison of experimental values of the electron density and the Laplacian at the bond critical points.

First line: bond length (l) (Å); second line: ρ_b (e Å^{-3}); third line: $\nabla^2\rho_b$ (eÅ^{-5}).

Bond		Bullvalene	Semibulvalene derivative	Barbaralane (I)
C1—C2	l	1.5352 (2)	1.5023 (10)	1.5035 (4)
	ρ_b	1.54 (1)	1.67 (4)	1.67 (2)
	$\nabla^2\rho_b$	−7.3 (1)	−7.7 (1)	−7.7 (1)
C2—C8	l	1.5352 (2)	1.6674 (12)	1.6495 (5)
	ρ_b	1.54 (1)	1.38 (3)	1.29 (1)
	$\nabla^2\rho_b$	−7.3 (1)	−1.0 (1)	−1.3 (1)
C2—C3	l	1.4727 (2)	1.4421 (10)	1.4658 (4)
	ρ_b	1.92 (1)	1.94 (5)	1.85 (2)
	$\nabla^2\rho_b$	−19.3 (1)	−18.0 (1)	−13.4 (1)
C3—C4	l	1.3450 (2)	1.3555 (12)	1.3529 (4)
	ρ_b	2.36 (2)	2.24 (5)	2.29 (2)
	$\nabla^2\rho_b$	−26.0 (1)	−20.1(2)	−19.5 (2)
C4—C5	l	1.5157 (2)	1.5193 (10)	1.5186 (4)
	ρ_b	1.78 (1)	1.84 (4)	1.68 (3)
	$\nabla^2\rho_b$	−16.0 (1)	−16.0 (2)	−7.7 (1)

The strain in the three-membered ring is clearly visible by the maxima outside the direct internuclear vectors indicating the bent character of the bonds in this region. The lowest density maximum is seen on the weaker bond C2—C8 that is considerably longer [d(C2—C8) = 1.6495 (5) Å] than the other two C—C bonds in the three-membered rings. In the C4—C5—C6 plane, the maxima of the charge density are on the internuclear vectors and there is no maximum between atoms C4 and C6 [d(C4—C6) = 2.4150 (4) Å].

The different C—C bond types in (I) were compared to related molecules like bullvalene (Koritsanszky *et al.*, 1996) and a semibullvalene derivative (Williams *et al.*, 1999), see Table 2. There is good agreement for ρ_b and $\nabla^2\rho_b$ on chemically related bonds, although these bonds are not fully identical due to differences in their geometry and attached substitution patterns. The bond orders for the different C—C bond types were calculated from the electron density at the bond critical points, making use of the relation

$$n = \exp[A(\rho_b - B)] \qquad (1)$$

proposed by Bader *et al.* (1983). The parameters A (1.02289) and B (1.64585) are obtained by fitting this function to the idealized single, double and triple bonds in ethane, ethylene and acetylene, using the B3LYP/6-31G* values for ρ_b (Table 3). As expected, the unsaturated bond (C3—C4) has the highest bond order. Because of conjugative interaction with the three-membered ring, the bond order for C2—C3 is higher than for a formal single bond. For the bond C2—C8, a bond order of $n < 1$ is obtained in theory as well as in experiment. This reflects the weak bond character of the long C—C bond in cyclopropane. However, the extrapolation to bond orders

Table 3
Bond order of the C—C bonds of 2,4,6,8-tetraphenylbarbaralane (I).

Bond	Bond order (experimental)	Bond order (theoretical)
C1—C2	1.02 (1)	1.02 (1)
C2—C8	0.69 (1)	0.63 (1)
C2—C3	1.23 (1)	1.23 (1)
C3—C4	1.89 (2)	1.89 (2)
C4—C5	1.03 (1)	1.06 (1)
C5—C9	0.97 (1)	0.98 (1)
C9—C1	1.11 (1)	1.09 (1)

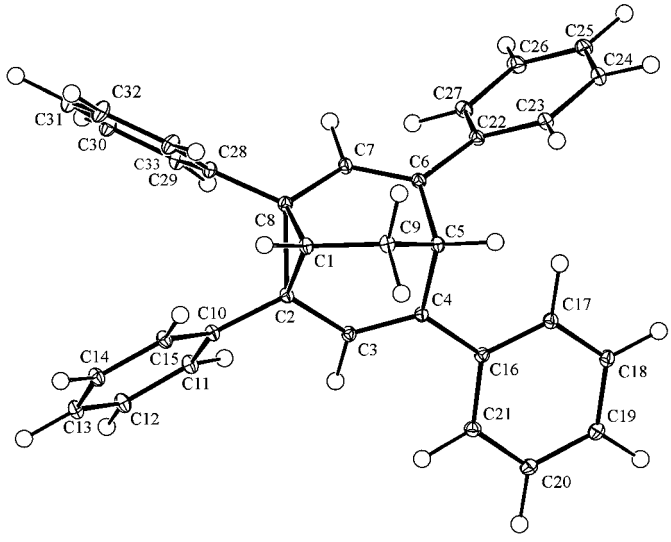

Figure 6
ORTEP (Burnett & Johnson, 1996) representation of (I) (50% probability) at 20 K with atomic numbering.

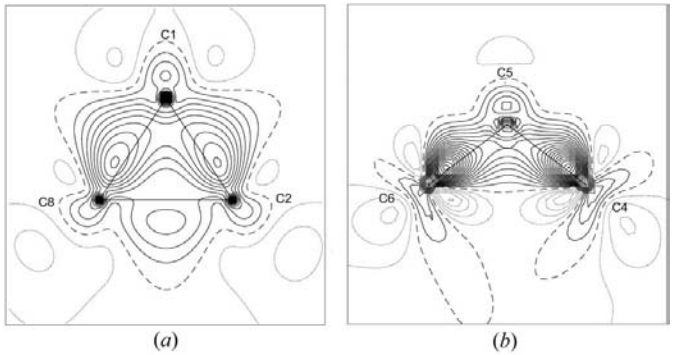

Figure 5
Deformation density map of the cyclopropane ring (*a*) and in the C4—C5—C6 plane of (I) (*b*) at 110 K.

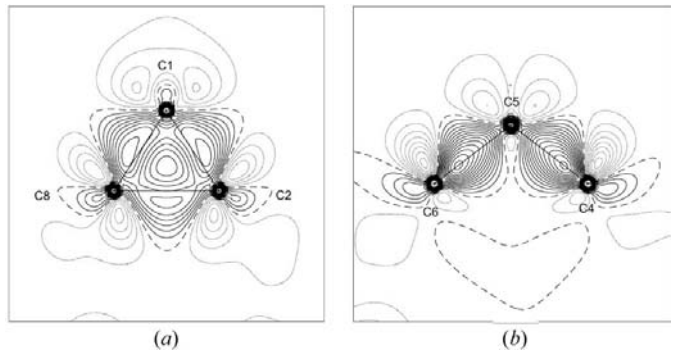

Figure 7
Deformation density map of the cyclopropane ring (*a*) and in the C4—C5—C6 plane of (I) (*b*) at 20 K.

smaller than one is uncertain because the extrapolation to zero bond order is not well defined.

Because we assumed that the disorder of the phenyl ring was a thermal effect, the substance was measured again with conventional X-radiation at 20 K. Owing to the comparatively low primary intensity, the measurement took several weeks. Reflections in the high-order region were found to be extremely weak. Attempting to add further runs in this region with exposure times of up to 4 min frame^{-1} gave no sufficient intensity yield, moreover the crystal decomposed in this period. Hence the laboratory set-up gave only a medium-resolution ($\sin\theta/\lambda$ = 0.9 Å^{-1}) data set compared to the 1.16 Å^{-1} resolution at the synchrotron beamline although the temperature was much lower. Fig. 6 shows an *ORTEP* (Burnett & Johnson, 1996) plot of the molecule (50% probability) based on the T = 20 K data

Space group; Z	$P\bar{1}$, triclinic; 1
Temperature (K)	100
Beamline	D3 (Hasylab)
Wavelength (Å)	0.56
$(\sin\theta/\lambda)_{max}$ (Å^{-1})	1.26
No. of collected refl.	365235
Symmetry ind. refl.	65891
R_{int}	0.061
R_W(F)	0.027

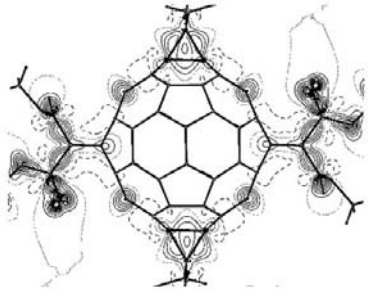

Figure 8
Synchrotron radiation was essential for the collection of a high-resolution data set of the fullerene derivative (II), see summary of the crystallographic data. Right: static deformation density map in an equator plane of the C_{60} sphere (from Wagner *et al.*, 2002).

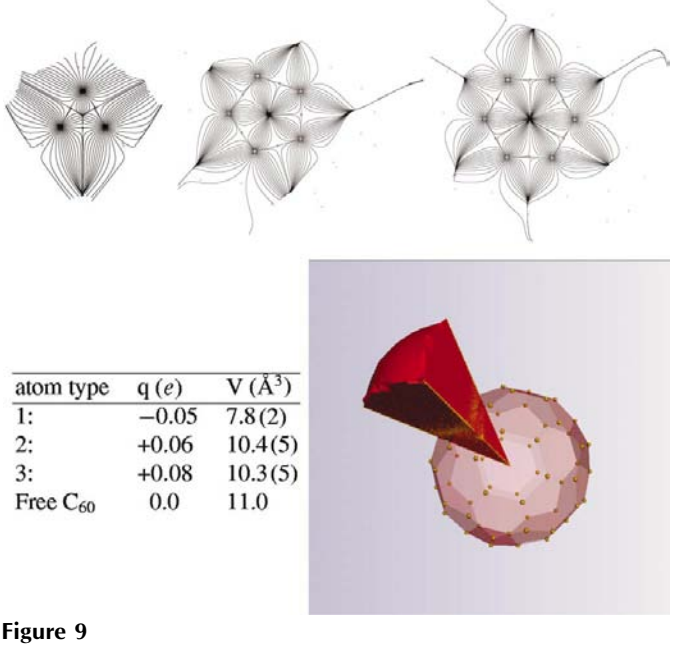

atom type	q (*e*)	V (Å^3)
1:	−0.05	7.8(2)
2:	+0.06	10.4(5)
3:	+0.08	10.3(5)
Free C_{60}	0.0	11.0

Figure 9
Top: gradient vector fields of the three-, five- and six-membered rings in the C_{60} derivative. Bottom left: their Bader charges and volumes. Bottom right: C-atom volume in free C_{60}. The limit for ρ_{min} is 0.001 a.u.

At 20 K, the disorder disappeared as shown in Fig. 7. The main features of the deformation density of the cyclopropane ring (*a*) and in the C4—C5—C6 plane (*b*) were comparable to the ones described in Fig. 5. Unfortunately, the corresponding experiment with synchrotron radiation at 20 K failed because of technical problems.

2.3. Atomic properties of a highly substituted C_{60} fullerene derivative (II)

Fullerenes are generally very unsuitable for experimental charge-density studies because of the poor quality of fullerene crystals and the high mobility of the molecules in the crystal lattice leading therefore to a strong intensity decrease with increasing diffraction angle.

In our attempt to collect a high-resolution data set, we examined unsuccessfully 18 different C_{60} derivatives, but finally we were able to grow suitable crystals of the highly substituted T_h-symmetrical derivative dodekakis(ethoxycarbonyl)-C_{60}-fullerene (II), $C_{102}H_{60}O_{24}$ (Lamparth *et al.*, 1995), which cocrystallized with 1,2-difluorobenzene (Fig. 8). Based on a data set of more than 350000 reflections measured in 5 d at 100 K up to a resolution of $\sin\theta/\lambda$ = 1.26 Å^{-1} at beamline D3 of Hasylab/DESY, we were able to derive a properly resolved charge-density distribution and related topological data, which were published earlier (Wagner *et al.*, 2002).

The partitioning procedure to obtain atomic regions makes use of the zero-flux surfaces in $\nabla\rho(\mathbf{r})$. It is available through the *TOPXD* program (Volkov *et al.*, 2000), which we could now apply to this problem. The results are illustrated in Fig. 9. Owing to the substitution, an exo cage three-membered ring is generated in addition to the five- and six-membered rings of the C_{60} sphere. Their gradient vector fields $\nabla\rho(\mathbf{r})$ are displayed in Fig. 9. While in the non-substituted I_h symmetrical C_{60} molecule all C atoms are equivalent, there are three chemi-

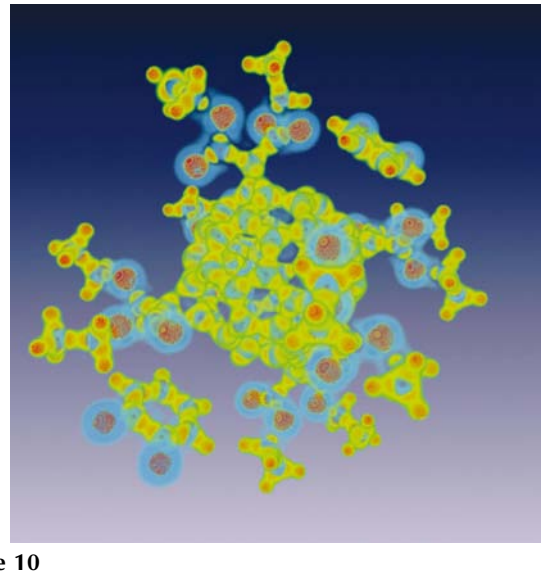

Figure 10
Volume rendering of the Laplace function of the fullerene derivative (II) cocrystallized with 1,2-difluorobenzene. For description of color code see text.

cally different C atoms in the C_{60} cage of this substituted derivative. A type 1 atom is involved in the cyclopropane ring formation, while type 2 and 3 atoms have different chemical environments on the C_{60} sphere (for details see Wagner *et al.*, 2002). The atomic properties volume and charge, summarized in Fig. 9, show that all 60 atoms of the fullerene moiety are practically uncharged. However, the volume of the type 1 atom is reduced by $\sim$2.5 Å^3 compared to the type 2 and 3 atoms, which have practically the same volume as found for the free C_{60}. The shape adopted for a single atom in C_{60} (derived from theory) is shown in Fig. 9. It originates at the sphere center and extends far beyond the molecular surface, if a cut-off of 0.001 a.u. is applied as is generally done for theoretically derived atomic volumes.

Carbon is known to exist with a large variety of atomic volumes. The volume of about 11 Å^3, exhibited by the C atoms on the C_{60} sphere, can be considered as a rather high value. We found a very small one, V = 4.1 Å^3, for a difluoro-substituted sp^3 C atom in octafluoro-1,2-dimethylenecyclobutane (Lentz *et al.*, 2003) that is even smaller than the carbon volume in diamond (V = 5.7 Å^3). Medium carbon volumes occur in cyclohexane (V = 8.5 Å^3) and graphite (V = 8.8 Å^3), while the 11 Å^3 volumes in C_{60} are somewhat smaller than in benzene (V = 12.3 Å^3). A very large C-atom volume was recently derived for an *sp*-hybridized C atom in acetylene dicyanide with V close to 20 Å^3 (Thieke, 2003).

The Laplacian of the charge density that is indicative for regions of charge accumulation [$\nabla^2\rho(\mathbf{r}) < 0$] and charge depletion [$\nabla^2\rho(\mathbf{r}) > 0$] is displayed in Fig. 10 as a volume rendering representation for the C_{60} derivative with the 1,2-difluorobenzene solvent molecule. Compared to isosurface plots, volume rendering has the advantage that continuous regions of the Laplacian can be visualized. Different colors in Fig. 10 represent different levels of the Laplacian, the interval for which the Laplacian is displayed ranges from -25 to $+25$ e Å^{-5}. Blue denotes positive values, negative values are from green to yellow to red. The highly accumulated charge is indicated in red, the accumulation in the bonds is shown as red, and blue halos around the electronegative O atoms denote a charge depletion around the atoms.

3. Conclusions

Stable beamline conditions provided, synchrotron radiation (at $\lambda\sim$ 0.5 Å) is the first choice for high-resolution charge-density data collection. This holds especially if smaller crystals are to be used (generally necessary for compounds with increasing molecular weight) with the added advantage of reduced absorption and extinction. Cooling to low temperatures around 20 K is superior to the normally applied 100 K cooling, since many significant high-order reflections that play an important role in charge-density data sets can be measured. However, for light-atom structures, provided crystals are large enough and diffract properly, Mo $K\alpha$ radiation can be sufficient, as was demonstrated by a data set of 220000 reflections collected in half a week with an Mo tube for the anti-thrombotic agent terbogrel containing more than 50 atoms (Flaig *et al.*, 2001).

A few drawbacks of synchrotron data collection should not be overlooked. One present technical problem is related to the dynamic range of the CCD detector and becomes especially critical for measurements at synchrotron beamlines. If a rather large crystal is chosen to enable the collection of high-order diffraction data, then several low-order reflections might be too strong in the bright synchrotron light and can no longer be integrated due to detector overload. This problem will surely be solved for future-generation area detectors. More severe is at present the narrow time scale of beam time periods, which is in some relation to the lack of beamlines directly conditioned for charge-density experiments. It is therefore good news that a dedicated charge-density beamline is in progress at the APS of Argonne National Laboratory thanks to the activities of P. Coppens's group. However, further worldwide activities should be initiated to provide more of the bright synchrotron light to the charge-density community.

This work was funded by BMBF, Förderkennzeichen 05 SM8KEA0 and various grants of the Deutsche Forschungsgemeinschaft, Förderkennzeichen LU 222/22-1/2, LU 222/24-1/2. The crystals of the barbaralane derivative were kindly provided by Professor H. Quast, Würzburg, Germany.

References

Arnold, W. D., Sanders, L. K., McMahon, M. T., Volkov, A. V., Wu, G., Coppens, P., Wilson, S. R., Godbout, N. & Oldfield, E. (2000). *J. Am. Chem. Soc.* **122**, 4708–4717.

Bader, R. F. W. (1990). *Atoms in Molecules. A Quantum Theory. The International Series of Monographs on Chemistry* 22. Oxford: Clarendon Press.

Bader, R. F. W., Slee, T. S., Cremer, D. & Kraka, E. (1983). *J. Am. Chem. Soc.* **105**, 5061–5068.

Burnett, M. N. & Johnson, C. K. (1996). *ORTEPIII*. Report ORNL-6895. Oak Ridge National Laboratory, Tennessee, USA.

Coppens, P., Abramov, Y., Carducci, M., Korjov, B., Novozhilova, I., Alhambra, C. & Pressprich, M. R. (1999). *J. Am. Chem. Soc.* **121**, 2585–2593.

Dauter, Z. (2002). *Acta Cryst.* A**58**, C4.

Destro, R., Roversi, P., Barzaghi, M. & Marsh, R. E. (2000). *J. Phys. Chem.* A**104**, 1047–1054.

Dittrich, B., Flaig, R., Koritsanszky, T., Krane, H.-G., Morgenroth, W. & Luger, P. (2000). *Chem. Eur. J.* **6**, 2582–2589.

Dittrich, B., Koritsanszky, T., Grosche, M., Scherer, W., Flaig, R., Wagner, A., Krane, H.-G., Kessler, H., Riemer, C., Schreurs, A. M. M. & Luger, P. (2002). *Acta Cryst.* B**58**, 721–727.

Dittrich, B., Scheins, S., Paulmann, C. & Luger, P. (2003). *J. Phys. Chem.* A**107**, 7471–7474.

Flaig, R., Koritsanszky, T., Dittrich, B., Wagner, A. & Luger, P. (2002). *J. Am. Chem. Soc.* **124**, 3407–3417.

Flaig, R., Koritsanszky, T., Soyka, R., Häming, L. & Luger, P. (2001). *Angew. Chem.* **40**, 355–359.

Gatti, C., Bianchi, R., Destro, R. & Merati, F. (1992). *J. Mol. Struct. (Theochem.)*, **255**, 409–433.

Koritsanszky, T., Buschmann, J. & Luger, P. (1996). *J. Phys. Chem.* **100**, 10547–10553.

Koritsanszky, T., Flaig, R., Zobel, D., Krane, H.-G., Morgenroth, W. & Luger, P. (1998). *Science*, **279**, 356–358.

Koritsanszky, T., Zobel, D. & Luger, P. (2000). *J. Phys. Chem. A*, **104**, 1549–1556.
Lamparth, I., Maichle-Mössmer, C. & Hirsch, A. (1995). *Angew. Chem.* **107**, 1755–1757.
Lentz, D., Patzschke, M., Bach, A., Scheins, S. & Luger, P. (2003). *Org. Biomol. Chem.* **1**, 409–414.
Matta, C. & Bader, R. F. W. (2000). *Proteins: Struct. Funct. Genet.* **40**, 310–329.
Matta, C. F. & Bader, R. F. W. (2002). *Proteins: Struct. Funct. Genet.* **48**, 519–538.
Matta, C. F. & Bader, R. F. W. (2003). *Proteins: Struct. Funct. Genet.* **52**, 360–399.
Messerschmidt, M., Meyer, M. & Luger, P. (2003). *J. Appl. Cryst.* **36**, 1452–1454.
Quast, H., Knoll, K. & von Schnering, H. G. (1993). *Chem. Ber.* **126**, 1047–1060.
Scheins, S., Dittrich, B., Messerschmidt, M., Paulmann, C. & Luger, P. (2004). *Acta Cryst.* B**60**, 184–190.
Thieke, J. (2003). Diploma thesis, Institute of Chemistry/Crystallography, FU Berlin, Germany.
Volkov, A., Gatti, C., Abramov, Y. & Coppens, P. (2000). *Acta Cryst.* A**56**, 252–258.
Wagner, A., Flaig, R., Dittrich, B., Schmidt, H., Koritsanszky, T. & Luger, P. (2004). *Chem. Eur. J.* **10**, 2977–2982.
Wagner, A., Flaig, R., Zobel, D., Dittrich, B., Bombicz, P., Strümpel, M., Luger, P., Koritsánszky, T. & Krane, H.-G. (2002). *J. Phys. Chem. A*, **106**, 6581–6590.
Williams, R. V. (2001). *Eur. J. Org. Chem.* pp. 227–235.
Williams, R. V., Gadgil, V. R., Luger, P., Koritsanszky, T. & Weber, M. (1999). *J. Org. Chem.* **64**, 1180–1190.
Zobel, D., Luger, P., Dreissig, W. & Koritsanszky, T. (1992). *Acta Cryst.* B**48**, 837–848.